Topological Effects Near Order-Disorder Transitions in Symmetric Diblock Copolymer Melts[†]

Tom Herschberg,[‡] Jan-Michael Y. Carrillo,[*,¶] Bobby G. Sumpter,[¶] Eleni Panagiotou,[*,§] and Rajeev Kumar[*,¶]

‡*Department of Computer Science and Engineering, University of Tennessee at Chattanooga, Chattanooga, Tennessee 37403, United States*

¶*Center for Nanophase Materials Sciences, Oak Ridge National Laboratory, Oak Ridge, Tennessee 37831, United States*

§*Department of Mathematics, University of Tennessee at Chattanooga,Chattanooga, Tennessee 37403, United States*

E-mail: carrillojy@ornl.gov; eleni-panagiotou@utc.edu; kumarr@ornl.gov

[†]This manuscript has been authored by UT-Battelle, LLC, under contract DE-AC05-00OR22725 with the US Department of Energy (DOE). The US government retains and the publisher, by accepting the article for publication, acknowledges that the US government retains a nonexclusive, paid-up, irrevocable, worldwide license to publish or reproduce the published form of this manuscript, or allow others to do so, for US government purposes. DOE will provide public access to these results of federally sponsored research in accordance with the DOE Public Access Plan (`http://energy.gov/downloads/doe-public-access-plan`.)

Abstract

The effects of polymer chain topology on the order-disorder transition of symmetric AB diblock copolymer melts are studied using coarse-grained molecular dynamics simulations. Specifically, we compared chain conformations near the lamellar-disordered transition in melts of symmetric (*i.e.*, 50-50) AB diblock copolymers of linear chains, rings and trefoil knots at the same chain lengths. The order (lamellar)-disorder transition temperature (ODT) and the domain sizes, both shifted to lower values with the introduction of topological constraints leading to the sequence: linear chains > rings > trefoil knots. Investigation of the polymer chain conformations in terms of their radii of gyration, their writhe values (a measure for the degree of intertwining of a chain around itself) and their Jones polynomials (a method to measure entanglement of curves) showed that linear chains and rings remained stretched while knots were stretched as well as tightened in disordered melts close to the lamellar-disorder transition. This work highlights chain topology as an important factor in affecting microphase separation in block copolymers.

Introduction

The effects of topology in macromolecular solutions and melts of polymer rings and knots have been widely investigated by a number of researchers.[1–11] These studies highlight the importance of topological constraints and other effects resulting from the absence of chain ends in affecting polymer structure and dynamics characterized by reduced hydrodynamic sizes of chains, elevated glass transition temperatures and lower melt viscosities of rings and knots in comparison with linear chains. Furthermore, topological effects have been used to devise strategies for tailoring material properties in polymer blends and block copolymers. These strategies are based on controlling morphology, modification of rheology, and control of degradation rate, where knots can protect segments of the chain.[12–17]

To synthesize molecules with special topologies, Monte Carlo (MC) sampling and molec-

ular dynamics (MD) simulations were used to survey accessible molecular knots,[18] which can be ring-expanded to form knotted polymer chains.[16,19,20] In general, polymer rings and knots are difficult to synthesize at high purities (and low dispersity) and large amounts or in polymer melt quantities.[16,19,21,22] Despite these challenges, block copolymers composed of chains with different topologies have been synthesized and characterized. For example, Hawker *et al.* found a 30% decrease of domain spacing compared to their linear analogues for lamellae forming diblock copolymers due to the smaller size of the rings.[12] Similarly, Epps *et al.* found, through X-ray reflectivity analyses of cyclic polystyrene-block-poly[oligo(ethylene glycol) methacrylate] thin film, 20% smaller domain spacings than their linear counterparts.[15] A more exotic bicyclic topology was investigated by Satoh *et al.*, through grazing incidence X-ray scattering analysis of films, which exhibited 70% reductions in domain spacing relative to their linear analogue.[14] In contrast to the experimentally observed reduced domain spacing of lamellae in the diblock copolymer rings, effects of topological constraints on the order-disorder transition as well as chain conformations near the transition remain poorly understood. To develop a better understanding, we use coarse-grained MD simulations to examine the effects of chain topology on the lamellar-disorder transition and chain conformations near the transition.

Due to inherent difficulties in considering topological constraints related to knots, some of the simplest knotted chain architectures such as trefoil knots are non-trivial to model using field theoretic methods such as the self consistent field theory (SCFT).[23,24] In this regard, particle based simulations such as MD and MC are attractive computational tools but require extensive computations.[13,15] In this paper, we present the effects of chain topology on the microphase separation in symmetric diblock copolymer melts using MD. Specifically, we determined the effects of a knotted topology (trefoil knot) on the order-disorder transition temperature, T_{ODT}, and how the transition was affected by topology of the diblock copolymer chains. To accomplish this, we compared several MD simulations of copolymer melts consisting of linear chains, rings and trefoil knots (3_1 in Alexander–Briggs notation).[25] We

considered rings and trefoil knots as these are the simplest experimentally[19] accessible chain topologies. Furthermore, to simplify matters, we limited our study to the lamellar morphology, which is expected for symmetric diblock copolymers (i.e., $f = 0.5$ volume fraction of A and B blocks) on the basis of symmetry.

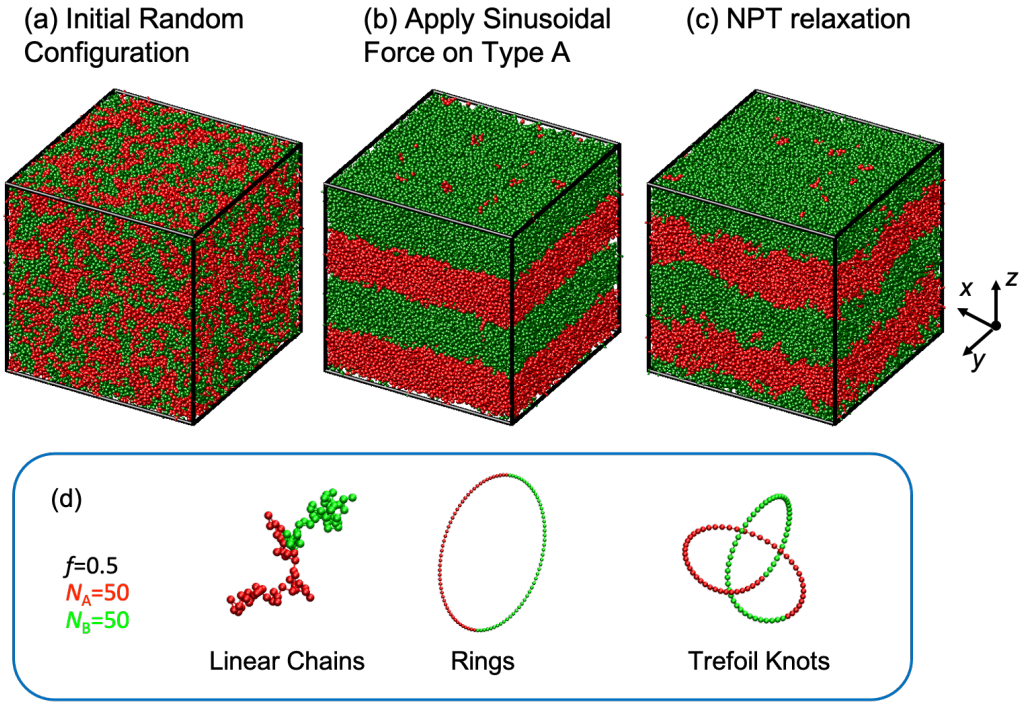

Figure 1: Simulation protocol: (a) diblock copolymers were randomly distributed, (b) a distance dependent force $f_z(z)$ was applied to induce a lamellar morphology with n number of domains, (c) NPT relaxation. The systems simulated were, $f = 0.5$ mole fraction, of 50 A-bead (red) and 50 B-bead (green) blocks of linear chains, rings or trefoil knots (d).

Simulation Details

Coarse-grained MD simulations were set-up by employing the interaction parameters designed for polystyrene (PS) and poly (methyl methacrylate) (PMMA) blends as described in the work by Chremos *et al.*[26] The polymer blocks were represented by connected Lennard-Jones (LJ) beads with characteristics size σ and interaction parameters, ϵ_{AA}, ϵ_{BB} and ϵ_{AB}. The bonds connecting the LJ beads were taken to be anharmonic FENE bonds,[27] which can maintain the topology of the diblock copolymer molecules due to their non-crossable

nature. Each chain contained 50 LJ beads in both A and B blocks with a total degree-of-polymerization, $N = 100$ in a simulation box containing 1000 chains. Snapshots of the simulation box and illustrations of the simulation protocol are shown in Figure 1.

The MD simulation protocol shown in Figure 1 involved three steps. First, the interaction parameters were initially set to purely repulsive between A-A, A-B and B-B beads to form a fully random and disordered melt (Figure 1(a)). Second, the interaction parameters were set to that of PS and PMMA, however, the A-B interaction parameter was kept as purely repulsive, while a distance dependent force, $f_z(z) = \cos(2\pi nz/L_z)k_BT/\sigma$, was applied to A beads, thereby biasing the system to form a lamella morphology that have n number of domains (Figure 1(b)). Here, L_z is the z dimension of the simulation box and k_BT is the thermal energy so that T is the temperature. The third step involves removing f_z and then letting the simulation box relax by running an isothermal-isobaric (NPT) ensemble run using a Langevin thermostat[28] and a Berendsen barostat[29] to maintain temperature and pressure, respectively (Figure 1(c)). As the value of number of lamellae domains (n) is not known *a priori* we scanned several values to determine the particular value of n where the lamellar morphology was maintained during relaxation while maintaining a cubic shape at $T = 1.00$ for linear chains and $T = 0.70$ for rings and trefoil knots. (See Figure S2 of the Supporting Information, SI.) Different sets of simulation runs for linear chains, rings and trefoil knots diblock copolymer melts at those specified temperatures and zero pressure were performed. We determined the values of n that correspond to our system size as $n = 2, 3$ and 3 for linear chains, rings, and trefoil knots, respectively. This initial set of simulations also allowed for an estimate on the box dimensions, hence, we repeated the simulations and considered different temperatures. These next sets of simulations were NPT ensemble simulations, where the x and y barostats were coupled and the z barostat was independent, equilibrating these systems and allowing them to change their shapes, thereby obtaining stress-free lamellar phases. Furthermore, to improve the statistics and increase the number of domains investigated, several simulations were further performed where the initial box

size in the z dimension, L_z of each system was either doubled, tripled or quadrupled relative to the previous simulation set; while their corresponding estimated number of domain were increased to $2n$, $3n$, and $4n$; and their initial L_x and L_y dimensions were reduced by factors of $1/\sqrt{2}$, $1/\sqrt{3}$ and $1/2$, respectively. The equilibrium box dimensions for the $1n$, $2n$, $3n$ and $4n$ simulation sets (designated as Set 1, Set 2, Set 3 and Set 4, respectively) are presented in Tables S1-S3. All results presented here were obtained from NPT runs where the parallel and normal barostats are decoupled. All simulations were performed using the LAMMPS[30,31] software package. See the SI for further details of the simulations.

Results and Discussion

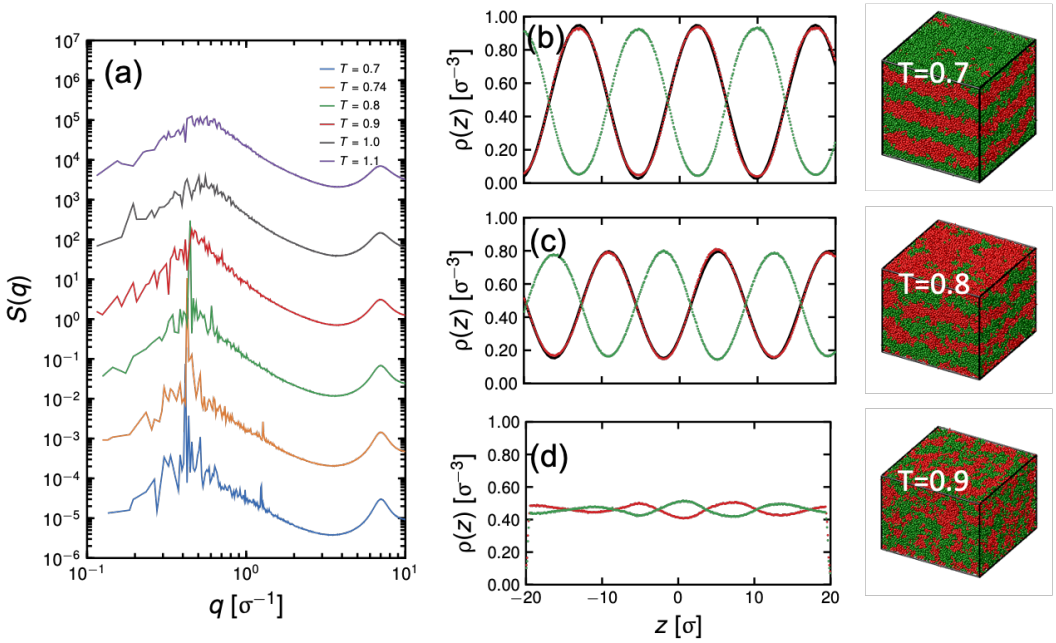

Figure 2: Scattering functions, $S(q)$, of A beads in diblock copolymer melts composed of trefoil knots at different temperatures (a). The functions were normalized such that $S(0) = 1$ and the $S(q)$ values were shifted for clarity by $\times 50^i$ where $i = \{0...5\}$ that pertains to the data set index number, *e.g.*, $T = 0.7$ and 1.1 has $i = 0$ and 5, respectively, where $T = 0.7$ is the unshifted curve. Density distribution, $\rho(z)$, at $T = 0.7$ (b), $T = 0.8$ (c), and $T = 0.9$ (d) of A beads (red dots) and B beads (green dots). The black line in (b-c) are fits to $\rho(z)$ of A beads. Snapshots of the melts are shown in the right.

To determine the order (lamellar)-disorder transition temperature (T_{ODT}), we monitored

the disappearance of the lamellar morphology as a function of temperature. We utilized both reciprocal and real-space approaches; scattering function, $S(q)$, and the density distribution, $\rho(z)$, of A and B beads in the z-direction (or normal to the lamellar planes), respectively. The $S(q)$ for A beads in the melts composed of trefoil knots shown in Figure 2(a) were obtained using the procedure by Carrillo and Dobrynin.[32] The $S(q)$ is the density-density correlation function of A beads and was obtained by performing 3D Fourier transform on the 3D density distribution of A beads. $S(q)$ can be expressed as $S(\vec{q}) = \frac{1}{n_s}\sum_{j=1}^{n_s}\sum_{k=1}^{n_s}\left\langle e^{-i\vec{q}(\vec{r}_j-\vec{r}_k)}\right\rangle$, and is defined as a sum over all pairs of n_s scatterers in the scattering volume, where $\vec{q}$ is the scattering wave vector and $\vec{r}_j$ is the position vector of the j^{th} scatterer.[33] The peak at high-q corresponds to the distance between A-beads while the sharp scattering peaks at low-q pertains to A domain length-scales. Sharp scattering peaks at low-q broadens for melts of trefoil knots at $T > 0.8$ which suggests the disappearance of domains. Further scrutinizing $\rho(z)$ at temperatures between $T = 0.7$ and $T = 0.9$ showed that the amplitude of the oscillations in $\rho(z)$ drastically decreased as T crossed this range (Figure 2(b-d)). Both approaches suggested $T_{ODT} \sim 0.8$ for the trefoil knot system. Similar analysis was done for the rings and linear diblock copolymers. Moreover, the $\rho(z)$ of the systems could be phenomenologically fitted with a function $\rho(z) \sim \cos^2(\pi z/D)$ to obtain D (see fits in Figure 2(b-c)), which is the characteristic domain spacing. The significance of D will be discussed later in the manuscript.

To understand effects of chain topology on the underlying conformational changes near the transition, we calculated the gyration tensor.[34] In Figure 3 (a-c), we plotted the dependence of the mean-square radius of gyration, $\left\langle R_g^2\right\rangle$, of linear chains, rings, and trefoil knots as a function of T. $\left\langle R_g^2\right\rangle$ was obtained by calculating the eigenvalues ($\lambda_j, j = 1, 2, 3$) of the gyration tensor and using $\left\langle R_g^2\right\rangle = \langle\lambda_1^2 + \lambda_2^2 + \lambda_3^2\rangle$. We observed a continuous transition, characterized by a rapid change of $\left\langle R_g^2\right\rangle$ with respect to T, where we designated T_{ODT} as the minimum of the plot $\frac{d\left\langle R_g^2\right\rangle}{dT}$ as shown in Figure S6(c). Alternatively, similar values of T_{ODT} were obtained by taking the minimum of $\frac{d\psi}{dT}$ where ψ is the inhomogeneity order

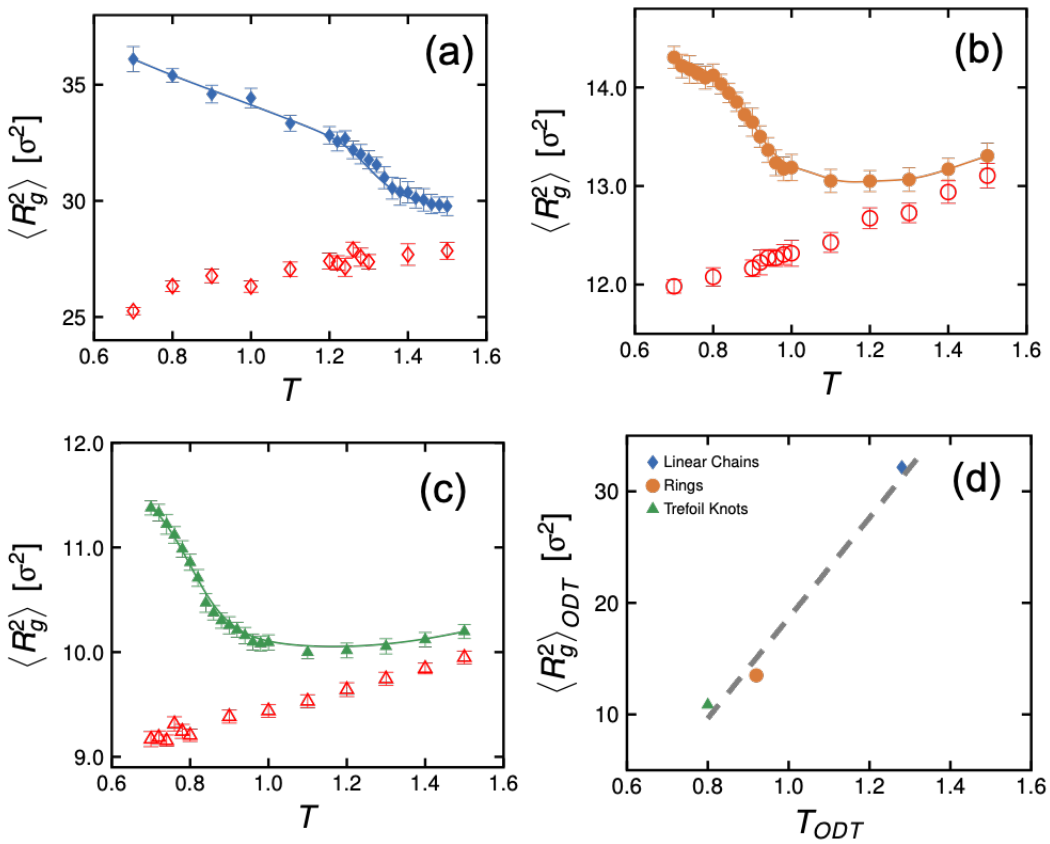

Figure 3: Mean-squared radius of gyration, $\langle R_g^2 \rangle$, of linear chains (a), rings (b) and trefoil knotted (c) diblock copolymers. The lines are spline fits. Red symbols corresponded to values of $\langle R_g^2 \rangle$ of linear homopolymers composed of type A beads of the same lengths as the copolymers. The correlation between $\langle R_g^2 \rangle$ and T_{ODT} are shown in (d). Dashed gray line is a guide to the eye.

parameter[35,36], and defined as $\psi = \langle [\rho_A(z) - \bar{\rho_A}]^2 + [\rho_B(z) - \bar{\rho_B}]^2 \rangle$, where $[\rho(z) - \bar{\rho}]^2$ is the squared difference of the local number density with the global number density of either A or B beads and $\langle ... \rangle$ is an ensemble average, as shown in Figure S6(a-b). We found the T_{ODT}'s as 1.28, 0.92 and 0.80 for linear chains, rings, and trefoil knots, respectively. Furthermore, all three systems showed higher values of $\left\langle R_g^2 \right\rangle$ relative to the homopolymers containing the same number of beads at lower temperatures, suggesting that the diblock chains were stretched at low temperatures, and approached the homopolymer size at higher temperatures. The chain stretching direction was found to be along normal to the lamellae interfaces (*i.e.*, along z-axis) as shown in Figures S8 and S9 in SI. Calculations of the average relative shape anisotropy $\langle \kappa^2 \rangle$ also support the stretching (see Figures S8 in SI). For $T \gg T_{ODT}$ (see Figure S9), the chains became isotropic so that $\left\langle R_{g,x}^2 \right\rangle \approx \left\langle R_{g,y}^2 \right\rangle \approx \left\langle R_{g,z}^2 \right\rangle$ and approach the size of the homopolymer chains, as expected. However, the chains remained stretched in the disordered phase at $T \simeq T_{ODT}$. Such a behavior has also been observed in the melts of linear diblock copolymer chains.[37] Furthermore, in Figure 3(d), we have shown that $\left\langle R_g^2 \right\rangle$ at ODT (which is proportional to the domain spacing of the lamellar morphology) is directly correlated with T_{ODT} confirming that the system free energy is a balance between enthalpic interaction, typically denoted by the Flory-Huggins χ_{AB} parameter, and conformational entropy of the chains.[38,39] Existence of such a correlation is expected on the basis of the random phase approximation (RPA) applied to the Gaussian diblock copolymer linear chains and rings. For example, the ODT's are estimated to be at $\chi_{AB}N = 10.49$ and 17.79 along with the domain spacing of the ordered morphology to be $D/(N_K^{1/2} l_K) = 1.32$ and 0.63 for linear[40] and ring[24,41] diblock copolymers, respectively, containing N_K Kuhn segments, each of length l_K.

We can compare the SCFT predictions and MD estimates of T_{ODT} by invoking a temperature dependence of the χ_{AB} parameters. For comparison purposes, we have used the mapping scheme devised by Chremos *et al.*[26] for Lennard-Jones chains to estimate χ_{AB}, which invoked $\chi_{AB} = \alpha/T + \beta$ such that $\alpha(\epsilon_{BB}, \epsilon_{AB}) = 9.8\epsilon_{BB} - 18.4\epsilon_{AB} + 8.6$ and $\beta(\epsilon_{BB}, \epsilon_{AB}) =$

$-4.6\epsilon_{BB} + 6.9\epsilon_{AB} - 2.4$. Such a temperature dependence of χ_{AB} led to the relation $T_{ODT} = \alpha N/[(\chi N)^{ODT} - \beta N]$. For the systems studied in this work ($\epsilon_{BB} = 0.9354, \epsilon_{AB} = 0.9312$) so that $\alpha = 0.633$ and $\beta = -0.278$, which led to $T_{ODT} = 1.654$ and $T_{ODT} = 1.390$ for linear chains ($(\chi N)^{ODT} = 10.49$) and rings ($(\chi N)^{ODT} = 17.79$), respectively, with each containing $N = 100$ Kuhn segments. Such a comparison revealed that the SCFT and MD predictions were in qualitative agreement but differ quantitatively. Another way to use the SCFT results was by including the effects of chain stretching near the order-disorder transition. (see Figure 3(d)) For such purposes, we used another procedure presented by Chremos *et al.*,[26] which led to the definition of an effective number of Kuhn segments representing a Lennard-Jones chain, $N_{eff} = N/s + 2$, where $s \simeq 2.6$ is a numerically estimated stretching ratio for linear symmetric diblock chains. This led to $T_{ODT} = \alpha/[(\chi N)^{ODT}/N_{eff} - \beta]$. Using $s \simeq 2.6$ for the rings also, we estimated $T_{ODT} = 1.179$ and $T_{ODT} = 0.882$ for linear chains and rings, respectively, each containing $N = 100$ Kuhn segments. This is in a better agreement with the MD results. This analysis shows that differences in the extent of stretching for linear chains and rings affect their order-disorder transition temperatures.

An analogy between rings containing N Kuhn segments and linear chains containing $N/2$ segments could be drawn for Gaussian chains in the strong stretching limit. A similar analogy could be drawn for Gaussian homopolymer chains.[42] However, such an analogy is not valid for *short chains* in the weak and the strong segregation limits (see Figure S7). For example, the validity of such an analogy would lead to an estimated $[\chi_{AB}N]^{ODT}_{rings} = 2\,[\chi_{AB}N]^{ODT}_{linear} = 20.99$ instead of 17.79 as predicted by the RPA (cf. Ref.[24]). Nevertheless, the chains in the MD simulations are short, which do not follow Gaussian chain statistics, and we have performed additional simulations to verify the validity of the analogy. Specifically, we simulated diblock linear chains with $N = 50$ and found that the linear chains stretched more in comparison with the $N = 100$ diblock copolymer rings *i.e.*, $\langle R_g^2 \rangle$ is higher (see Figure S7). These differences in chain stretching led to differences in domain spacing D of the lamellar morphology in the case of rings (*i.e.*, $D_{rings,N=100} > D_{linear,N=50}$, see Figure S10) and $T_{ODT,rings,N=100} >$

$T_{ODT,linear,N=50}$ (see Figure S6). These results clearly show that the analogy between rings and linear chains is not valid for the weak segregation limit. Furthermore, these additional results show that constraints due to the chain ends play a significant role in stabilizing homogeneous phase over an inhomogeneous phase such as lamellar.

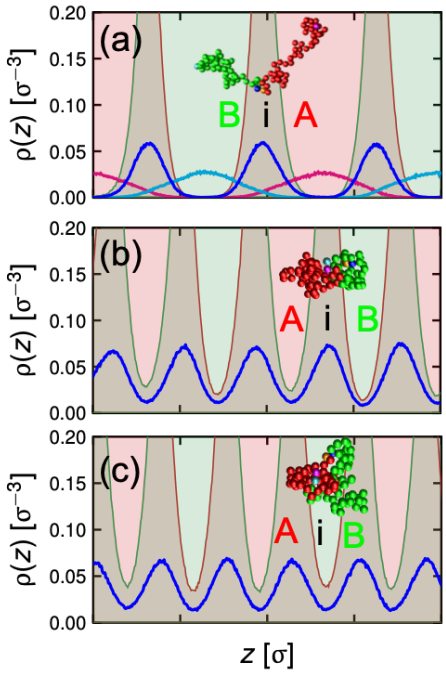

Figure 4: Density distributions of free ends of block A (magenta line), free ends of block B (cyan line) and junction beads (blue line) of linear chains (a); and the density distributions of junction beads for rings (b) and trefoil knots (c) (blue line) of diblock copolymer melts at $T = 0.7$. The filled red (A), brown (i), and green (B) regions refer to the A-domains, interfacial regions, and B-domains in (a), (b) and (c), respectively. Typical configurations of the diblock copolymer molecules are shown in the inserts. These figures show that junctions populate the interfacial regions (shown as magenta, cyan, blue and orange beads in the inserts of (b) and (c) and only blue and orange beads in the insert of (a)), independent of the chain topology.

In the strong segregation limit (low T), characterized by narrow interfacial regions, the junction points in linear block copolymers are expected to be situated at the interface.[35,38] In Figure 4(a), we calculated the density distributions of the 1^{st} and last beads of both A and B blocks of the melts of linear chains and superimposed these densities onto the total number densities of A and B. The free ends of the chain are mostly found in the middle of their respective domains, while the junction points are found in the interfacial region (or **i** in

Figure 4) resulting in an out-of-phase sinusoidal pattern for chain ends of A and B blocks. We repeated the same procedure for the rings and trefoil knots systems (Figure 4(b-c)), and we observed similar sinusoidal patterns for all monitored beads. That is, all the junction points between A and B blocks were situated in the interfacial region independent of the chain topology.

The main difference between the rings and the trefoil knots systems lies in the presence of the tangled loops, which can be quantified by calculating the writhe, W_r, of the curve.[43–45] In the context of melts of linear polymer chains, the mean absolute writhe, $\langle|W_r|\rangle$, which is a global measure of self-entanglement of a chain, was used to estimate the number of monomers in an entanglement strand[46] and quantify the relationship between polymer chain entanglement and viscoelastic responses.[47] As a reference, the $\langle|W_r|\rangle$ values for the homopolymer melts composed of linear chains, rings, and trefoil knots at $T = 1.0$ were calculated and were found to be $\sim 1.26, 1.42$ and 3.49, respectively. The magnitude of $\langle|W_r|\rangle$ is a measure of how intertwined a curve is with itself, with higher magnitudes, on average, pointing to a curve with more intertwining loops. Thus the homopolymer trefoil knot is the most intertwined among the three topologies, as expected.

In Figure 5, the $\langle|W_r|\rangle$ of the diblock copolymer is compared with its homopolymer counterpart, and for linear chains and rings, the $\langle|W_r|\rangle$ of the homopolymer is larger than that of the diblock copolymer. This behavior is expected since the writhe gives on average a smaller absolute value for more extended or stretched configurations of unknotted curves.[48,49] The sketch representation in Figure 5(a) illustrates that for a linear chain, a stretched configuration of diblock chains are less intertwined than that of the near random-walk conformation of homopolymer melts. The situation is similar (Figure 5(b)) to those in diblock rings and homopolymer rings, although there is more intertwining for stretched rings than stretched linear copolymer chains. However, this is opposite to what is observed in trefoil knots (Figure 5(c)), where the $\langle|W_r|\rangle$ is larger in diblock copolymers despite having a more extended configuration at low T. This may be a result of the knot tightening upon stretching. Also,

we observed that $\langle|W_r|\rangle$ of diblock copolymers and homopolymers approach a similar value at high T.

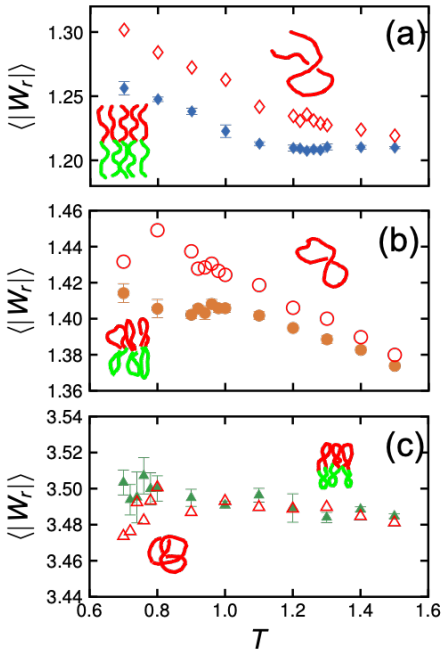

Figure 5: Mean absolute writhe $\langle|W_r|\rangle$, of linear chains (a), rings (b) and trefoil knots (c). Open red symbols are for homopolymers while filled symbols are for diblock copolymers. Sketches depict representative configurations of the diblock and homopolymer chains.

Next, we obtained the $\langle|W_r|\rangle$ of the A and B blocks of the diblock copolymer by calculating the writhe from 1^{st} to 50^{th} bead (A-block) and 51^{st} to 100^{th} bead (B-block), and for reference, we repeated the same calculation for the homopolymers. (See Figure S11). We observed that $\langle|W_r|\rangle_A > \langle|W_r|\rangle_B$ in the diblock copolymer system, which can be attributed to a denser packing of A monomers since $\epsilon_{AA} > \epsilon_{BB}$ for the LJ pairwise interactions. For a melt of homopolymer chains composed of A beads, $\langle|W_r|\rangle_A^{1-50} \approx \langle|W_r|\rangle_A^{51-100}$, where the superscripts represent the range of bead indices in the homopolymers and presented as the average value in Figure S11. Despite the blocks being more extended relative to the homopolymers, the $\langle|W_r|\rangle$ of blocks A and B is greater than those of their homopolymer counterparts suggesting that self-intertwining of these blocks are evident in the lamellar morphology and is the most apparent in the trefoil knots. This can be further visualized by investigating the normalized writhe in Figure 6 which shows a noticeable difference for the trefoil knots at temperatures

below T_{ODT} — an indication of the tightening of intertwined parts of the permanent knot in a trefoil knotted chain.

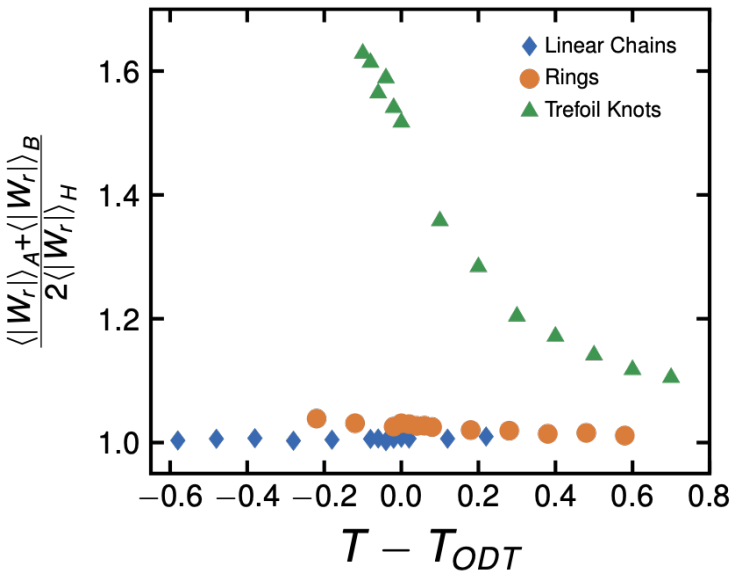

Figure 6: Normalized absolute mean writhe, $\frac{\langle|W_r|\rangle_A+\langle|W_r|\rangle_B}{2\langle|W_r|\rangle_H}$, of individual blocks in linear chains, rings and trefoil knots in comparison with homopolymers (H) of the same chain topology as the diblock copolymers. An increase in the absolute mean writhe for the trefoil knotted copolymers on lowering the temperature signifies tightening of intertwined parts.

In order to examine more accurately how the configurations of the knotted chains change as a function of temperature, we use the recently discovered Jones polynomial of open chains (see[50] and references therein). The Jones polynomial is a stronger measure of entanglement than the writhe of a chain, since it can detect different knot types.[51,52] However, its complex definition and the fact that, until recently, it was rigorously defined only for ring polymers (and not for linear chains) did not allow for its extensive application to polymer melts and solutions. Nevertheless, it has been applied to ring polymers to successfully provide an estimator of the entanglement length in Ref.[53] Studies of proteins and other biopolymers have shown that knot polynomials (upon artifical closure of macromolecules) are useful in characterizing their conformation.[54–58] Here, we used the Jones polynomial of open chains, which can detect knots in open segments without requiring any artificial closures.[50] For more details see Section 1.8 in SI. By scanning along each chain at different length scales

and calculating the Jones polynomial at each segment, we can detect the shortest segment of a chain that ties the trefoil knot. Figure 7 shows the analysis of the location and length of the trefoil knot within a chain as a function of T. We see that the percentage of chains for which the trefoil has length larger than half of the length of a chain is increasing with temperature. The distribution of knot lengths (see Figure S12) shows that there are more tighter knots (shorter length) at lower temperatures. Similarly, we see that the percentage of chains with the knot consisting of both A and B blocks is increasing with temperature. For $T < T_{ODT}$, most of the trefoils lie entirely in blocks A and B with the majority of those in block A. At $T \approx T_{ODT}$ we see a transition to trefoil knots containing both A and B block segments. This suggests that the location of the knot within an AB diblock polymer is important for the order-disorder transition. At $T \approx 0.8$, we also see an increase of the percentage of the trefoil knots of more than 50 monomers, suggesting that the knots loosen up with an increase in temperature. Our results also show that the percentage of trefoils lying entirely within block A is greater than the percentage of trefoils lying entirely within block B at all temperatures. This shows that the attractive interaction influences knottedness significantly.

We propose that the presence of permanent knots, as a result of the chain topology, reduces entropy of the melt since knots prevent a chain from acquiring various possible conformations available for an unknotted chain. Such a reduction in configurational entropy due to topological constraints causes a shift of the T_{ODT} to lower temperatures. Further evidence of this reduction due to topological constraints is seen in the trend of domain spacing, D as a function of T (see Figure 8), where $D/\left\langle R_g^2 \right\rangle^{1/2}$ are generally higher for trefoil knots despite having lower values of D (see Figure S10). Furthermore, the results shown in Figure 8 qualitatively agree with experiments[12,14,15] and show the expected proportionality of radius of gyration, $\left\langle R_g^2 \right\rangle^{1/2}$ of the blocks with the lamellar domains spacing, D.

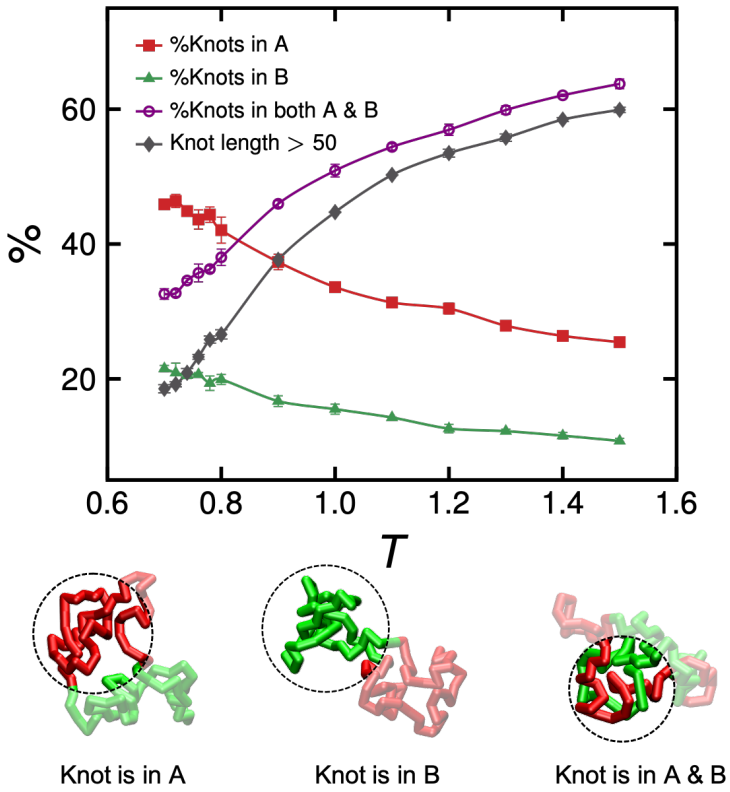

Figure 7: Analysis of the location and length of the trefoil knot within a knotted copolymer chain as a function of T. Images in the bottom-left, -middle and -right are typical knot configurations made up of A beads, B beads and both A & B beads, respectively.

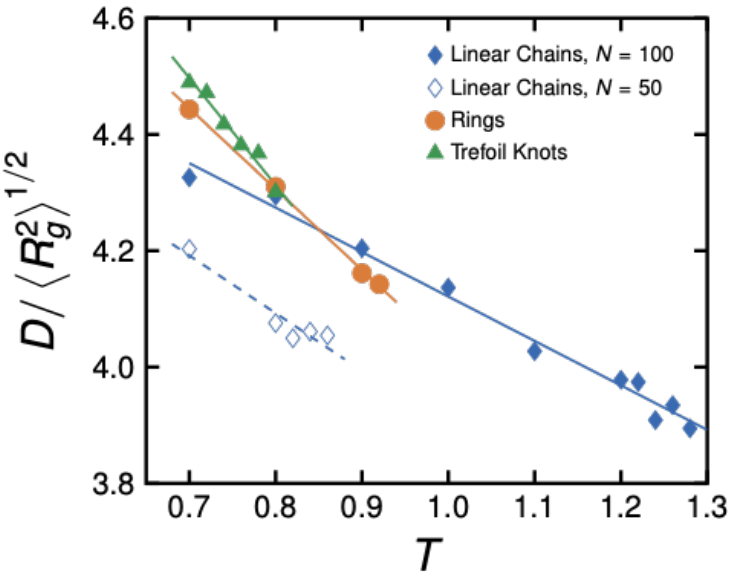

Figure 8: The ratio of the domain spacing and radius of gyration, $D/\left\langle R_g^2 \right\rangle^{1/2}$, for linear chains, rings and trefoil knots diblock copolymer melts as a function of T. Lines are linear fits.

Conclusions

In summary, we have found that topological effects resulting from the absence of chain ends and knotted topology are significant in shifting the lamellar-disordered transition to lower temperatures along with a decrease of the length scale appearing at the transition. The chains are found to be stretched normal to the lamellae interfaces and in the disordered phase near the transition independent of the chain topology. Furthermore, the junctions enrich the interfaces and the writhe values of trefoil knots increase in magnitude along with chains being stretched in the lamellar morphology. The transition to lamellar morphology occurs when the knot tightens and lies in one of the two blocks, which is determined by the interaction parameters within the blocks. Overall, this work shows that macromolecular chain topology is an important factor affecting microphase separation in block copolymer melts.

Acknowledgement

This work was performed at the Center for Nanophase Materials Sciences, a US DOE Office of Science User Facility. This research used resources of the Oak Ridge Leadership Computing Facility (OLCF) and of the Compute and Data Environment for Science (CADES) at the Oak Ridge National Laboratory, which is supported by the Office of Science of the U.S. Department of Energy under Contract No. DE-AC05-00OR22725. TH and EP thank the support of NSF DMS #1913180.

Supporting Information Available

The Supporting Information is available free of charge at https://pubs.acs.org.

Simulation details and results; Figures S1–S12; Supporting references.

References

(1) Vargas-Lara, F.; Hassan, A. M.; Mansfield, M. L.; Douglas, J. F. Knot Energy, Complexity, and Mobility of Knotted Polymers. *Sci. Rep.* **2017**, *7*, 1–15.

(2) Douglas, J. F.; Vargas-Lara, F. Topological Rigidification of Flexible Polymers in Solution. AIP Conf. Proc. 2018; p 020005.

(3) Liebetreu, M.; Ripoll, M.; Likos, C. N. Trefoil Knot Hydrodynamic Delocalization on Sheared Ring Polymers. *ACS Macro Letters* **2018**, *7*, 447–452.

(4) Vargas-Lara, F.; Pazmiño Betancourt, B. A.; Douglas, J. F. Influence of Knot Complexity on Glass-Formation in Low Molecular Mass Ring Polymer Melts. *J. Chem. Phys.* **2019**, *150*, 101103.

(5) Weiss, L. B.; Marenda, M.; Micheletti, C.; Likos, C. N. Hydrodynamics and Filtering of Knotted Ring Polymers in Nanochannels. *Macromolecules* **2019**, *52*, 4111–4119.

(6) Zhang, T.; Winey, K. I.; Riggleman, R. A. Conformation and Dynamics of Ring Polymers under Symmetric Thin Film Confinement. *J. Chem. Phys.* **2020**, *153*, 184905.

(7) Mei, B.; Dell, Z. E.; Schweizer, K. S. Microscopic Theory of Long-Time Center-of-Mass Self-Diffusion and Anomalous Transport in Ring Polymer Liquids. *Macromolecules* **2020**, *53*, 10431–10445.

(8) Guo, F.; Li, K.; Wu, J.; He, L.; Zhang, L. Effects of Topological Constraints on Penetration Structures of Semi-Flexible Ring Polymers. *Polymers* **2020**, *12*, 2659.

(9) Landuzzi, F.; Nakamura, T.; Michieletto, D.; Sakaue, T. Persistence Homology of Entangled Rings. *Phys. Rev. Res.* **2020**, *2*, 033529.

(10) Jeong, S. H.; Cho, S.; Roh, E. J.; Ha, T. Y.; Kim, J. M.; Baig, C. Intrinsic Surface Characteristics and Dynamic Mechanisms of Ring Polymers in Solution and Melt Under Shear Flow. *Macromolecules* **2020**, *53*, 10051–10060.

(11) Pasquino, R.; Vasilakopoulos, T. C.; Jeong, Y. C.; Lee, H.; Rogers, S.; Sakellariou, G.; Allgaier, J.; Takano, A.; Brás, A. R.; Chang, T.; Gooßen, S.; Pyckhout-Hintzen, W.; Wischnewski, A.; Hadjichristidis, N.; Richter, D.; Rubinstein, M.; Vlassopoulos, D. Viscosity of Ring Polymer Melts. *ACS Macro Lett.* **2013**, *2*, 874–878.

(12) Poelma, J. E.; Ono, K.; Miyajima, D.; Aida, T.; Satoh, K.; Hawker, C. J. Cyclic Block Copolymers for Controlling Feature Sizes in Block Copolymer Lithography. *ACS nano* **2012**, *6*, 10845–10854.

(13) Goodson, A. D.; Troxler, J. E.; Rick, M. S.; Ashbaugh, H. S.; Albert, J. N. Impact of Cyclic Block Copolymer Chain Architecture and Degree of Polymerization on Nanoscale Domain Spacing: A Simulation and Scaling Theory Analysis. *Macromolecules* **2019**, *52*, 9389–9397.

(14) Ree, B. J.; Satoh, Y.; Isono, T.; Satoh, T. Bicyclic Topology Transforms Self-Assembled Nanostructures in Block Copolymer Thin Films. *Nano Letters* **2020**, *20*, 6520–6525.

(15) Gartner III, T. E.; Kubo, T.; Seo, Y.; Tansky, M.; Hall, L. M.; Sumerlin, B. S.; Epps III, T. H. Domain Spacing and Composition Profile Behavior in Salt-Doped Cyclic vs Linear Block Polymer Thin Films: A Joint Experimental and Simulation Study. *Macromolecules* **2017**, *50*, 7169–7176.

(16) Cao, P.-F.; Rong, L.-H.; Mangadlao, J. D.; Advincula, R. C. Synthesizing a Trefoil Knotted Block Copolymer via Ring-Expansion Strategy. *Macromolecules* **2017**, *50*, 1473–1481.

(17) Borger, A.; Wang, W.; O'Connor, T. C.; Ge, T.; Grest, G. S.; Jensen, G. V.; Ahn, J.; Chang, T.; Hassager, O.; Mortensen, K.; Vlassopoulos, D.; Huang, Q. Threading–Unthreading Transition of Linear-Ring Polymer Blends in Extensional Flow. *ACS Macro Lett.* **2020**, *9*, 1452–1457.

(18) Marenda, M.; Orlandini, E.; Micheletti, C. Discovering Privileged Topologies of Molecular Knots with Self-Assembling Models. *Nat. Commun.* **2018**, *9*, 1–8.

(19) Cao, P.-F.; Mangadlao, J.; Advincula, R. A Trefoil Knotted Polymer Produced through Ring Expansion. *Angewandte Chemie* **2015**, *127*, 5216–5220.

(20) Chang, Y. A.; Waymouth, R. M. Recent Progress on the Synthesis of Cyclic Polymers via Ring-Expansion Strategies. *Journal of Polymer Science Part A: Polymer Chemistry* **2017**, *55*, 2892–2902.

(21) Isono, T.; Sasamori, T.; Honda, K.; Mato, Y.; Yamamoto, T.; Tajima, K.; Satoh, T. Multicyclic Polymer Synthesis through Controlled/Living Cyclopolymerization of α, ω-Dinorbornenyl-Functionalized Macromonomers. *Macromolecules* **2018**, *51*, 3855–3864.

(22) Satoh, Y.; Matsuno, H.; Yamamoto, T.; Tajima, K.; Isono, T.; Satoh, T. Synthesis of Well-Defined Three-and Four-Armed Cage-Shaped Polymers via "Topological Conversion" from Trefoil-and Quatrefoil-Shaped Polymers. *Macromolecules* **2017**, *50*, 97–106.

(23) Zhang, J.; Wu, J.; Jiang, R.; Wang, Z.; Yin, Y.; Li, B.; Wang, Q. Lattice Self-Consistent Field Calculations of Confined Symmetric Block Copolymers of Various Chain Architectures. *Soft Matter* **2020**, *16*, 4311–4323.

(24) Kim, J. U.; Yang, Y.-B.; Lee, W. B. Self-Consistent Field Theory of Gaussian Ring Polymers. *Macromolecules* **2012**, *45*, 3263–3269.

(25) Alexander, J. W.; Briggs, G. B. On Types of Knotted Curves. *Ann. Math.* **1926**, 562–586.

(26) Chremos, A.; Nikoubashman, A.; Panagiotopoulos, A. Z. Flory-Huggins Parameter χ, from Binary Mixtures of Lennard-Jones Particles to Block Copolymer Melts. *J. Chem. Phys.* **2014**, *140*, 054909.

(27) Kremer, K.; Grest, G. S. Dynamics of Entangled Linear Polymer Melts: A Molecular-Dynamics Simulation. *J. Chem. Phys.* **1990**, *92*, 5057–5086.

(28) Schneider, T.; Stoll, E. Molecular-Dynamics Study of a Three-Dimensional One-Component Model for Distortive Phase Transitions. *Phys. Rev. B* **1978**, *17*, 1302.

(29) Berendsen, H. J.; Postma, J. v.; van Gunsteren, W. F.; DiNola, A.; Haak, J. R. Molecular Dynamics with Coupling to an External Bath. *J. Chem. Phys.* **1984**, *81*, 3684–3690.

(30) Plimpton, S. Fast Parallel Algorithms for Short-Range Molecular Dynamics. *J. Comput. Phys.* **1995**, *117*, 1–19.

(31) Brown, W. M.; Wang, P.; Plimpton, S. J.; Tharrington, A. N. Implementing Molecular Dynamics on Hybrid High Performance Computers–Short Range Forces. *Comput. Phys. Commun.* **2011**, *182*, 898–911.

(32) Carrillo, J.-M. Y.; Dobrynin, A. V. Polyelectrolytes in salt solutions: Molecular dynamics simulations. *Macromolecules* **2011**, *44*, 5798–5816.

(33) Rubinstein, M.; Colby, R. *Polymer Physics*; OUP Oxford, 2003.

(34) Theodorou, D. N.; Suter, U. W. Shape of Unperturbed Linear Polymers: Polypropylene. *Macromolecules* **1985**, *18*, 1206–1214.

(35) Li, W.; Carrillo, J.-M. Y.; Sumpter, B. G.; Kumar, R. Modulating Microphase Separation of Lamellae-Forming Diblock Copolymers via Ionic Junctions. *ACS Macro Letters* **2020**, *9*, 1667–1673.

(36) Kumar, R.; Li, W.; Sumpter, B. G.; Muthukumar, M. Understanding the Effects of Dipolar Interactions on the Thermodynamics of Diblock Copolymer Melts. *J. Chem. Phys.* **2019**, *151*, 054902.

(37) Almdal, K.; Rosedale, J. H.; Bates, F. S.; Wignall, G. D.; Fredrickson, G. H. Gaussian-to Stretched-Coil Transition in Block Copolymer Melts. *Phys. Rev. Lett.* **1990**, *65*, 1112.

(38) Bates, F. S.; Fredrickson, G. H. Block Copolymer Thermodynamics: Theory and Experiment. *Annu. Rev. Phys. Chem.* **1990**, *41*, 525–557.

(39) Helfand, E.; Wasserman, Z. R. Block Copolymer Theory. 4. Narrow Interphase Approximation. *Macromolecules* **1976**, *9*, 879–888.

(40) Leibler, L. Theory of Microphase Separation in Block Copolymers. *Macromolecules* **1980**, *13*, 1602–1617.

(41) Marko, J. Microphase Separation of Block Copolymer Rings. *Macromolecules* **1993**, *26*, 1442–1444.

(42) Casassa, E. F. Some Statistical Properties of Flexible Ring Polymers. *J. Poly. Sci. A.* **1965**, *3*, 605–614.

(43) Klenin, K.; Langowski, J. Computation of Writhe in Modeling of Supercoiled DNA. *Biopolymers.* **2000**, *54*, 307–317.

(44) Fuller, F. B. The Writhing Number of a Space Curve. *Proc. Natl. Acad. Sci. U.S.A.* **1971**, *68*, 815–819.

(45) Vologodskii, A. V.; Anshelevich, V. V.; Lukashin, A. V.; Frank-Kamenetskii, M. D. Statistical Mechanics of Supercoils and the Torsional Stiffness of the DNA Double Helix. *Nature* **1979**, *280*, 294–298.

(46) Panagiotou, E.; Kröger, M.; Millett, K. C. Writhe and Mutual Entanglement Combine to Give the Entanglement Length. *Phys. Rev. E* **2013**, *88*, 062604.

(47) Panagiotou, E.; Millett, K. C.; Atzberger, P. J. Topological Methods for Polymeric Materials: Characterizing the Relationship between Polymer Entanglement and Viscoelasticity. *Polymers* **2019**, *11*, 11030437.

(48) Panagiotou, E.; Kröger, M. Pulling-Force-Induced Elongation and Alignment Effects on Entanglement and Knotting Characteristics of Linear Polymers in a Melt. *Phys. Rev. E* **2014**, *90*, 042602.

(49) Rawdon, E. J.; Kern, J. C.; Piatek, M.; Plunkett, P.; Stasiak, A.; Millett, K. C. Effect of Knotting on the Shape of Polymers. *Macromolecules* **2008**, *41*, 8281–8287.

(50) Panagiotou, E.; Kauffman, L. Knot Polynomials of Open and Closed Curves. *Proc. R. Soc. A* **2020**, *476*, 20200124.

(51) Jones, V. A Polynomial Invariant of Knots via von Neumann Algebras. *Bull. Am. Math. Soc.* **1985**, *12*, 103–112.

(52) Jones, V. Hecke Algebra Representations of Braid Groups and Link Polynomials. *Ann. Math.* **1987**, *126*, 335–388.

(53) Qin, J.; Milner, S. T. Counting Polymer Knots to Find the Entanglement Length. *Soft Matter* **2011**, *7*, 10676–93.

(54) Millett, K. C.; Sheldon, B. Tying down open knots. *Series of Knots and Evereything* **2005**, *36*, 203–217.

(55) Sulkowska, J. I.; Rawdon, E. J.; Millett, K. C.; Onuchic, J. N.; Stasiak, A. Conservation of complex knotting and slpiknotting in patterns in proteins. *PNAS* **2012**, *109*, E1715.

(56) Virnau, P.; Mirny, L.; Kardar, M. Intricate Knots in Proteins: Function and Evolution. *PNAS* **2006**, *2*, e133.

(57) Coronel, L.; Suma, A.; Micheletti, C. Dynamics of Supercoiled DNA with Complex Knots: Large-Scale Rearrangements and Persistent Multi-Strand Interlocking. *Nucl. Acids Res.* **2018**, *46*, 7533–7541.

(58) C., L. R.; Grosberg, A. Y. Statistics of Knots, Geometry of Conformations, and Evolution of Proteins. *PLOS Comp. Biol.* **2006**, *2*, e45.
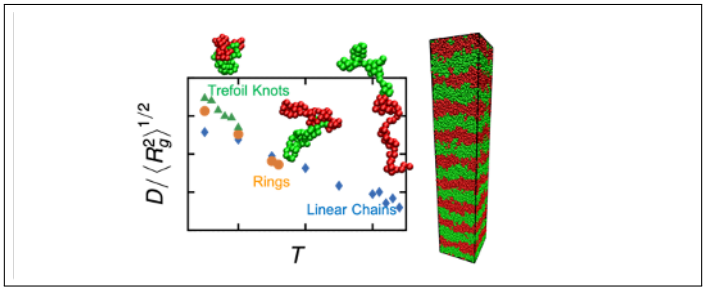
Graphical TOC Entry